ZIBELINE INTERNATIONAL PUBLISHING

ISSN: 1024-1752 (Print)

CODEN: JERDFO

Journal of Mechanical Engineering Research & Developments (JMERD)

***DOI** : http://doi.org/10.26480/jmerd.01.2019.26.33*

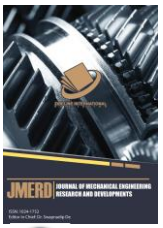

RESEARCH ARTICLE

DRAG INVESTIGATION AROUND A CYLINDER AND SYMMETRIC AIRFOIL IN TANDEM WITH DIFFERENT GAPS AND ANGLES OF ATTACK

Humam M. Salih, Mustafa A. Abdulhussain

Mechanical Engineering Department, University of Technology, Iraq.
***Corresponding Author Email:** humsalih2@gmail.com, mustafa_ahmed2018@yahoo.com*

ARTICLE DETAILS

Article History:

Received 20 November 2018
Accepted 26 December 2018
Available online 22 January 2019

ABSTRACT

A Numerical simulation for the turbulent airflow around a symmetrical airfoil (NACA 0012) adjusted in tandem with circular cylinder, the airfoil were adjusted at variable angle of attack between (5-20°) with positive clockwise inclination setting the cylinder center in front of the leading-edge centroid using the realizable K-ε turbulent model in the ANSYS FLUENT 17 package is performed. The effect of changing the adjusted tandem bodies' configuration, gap (0.05-0.1) and the cylinder size variation on the flow pressure distribution and the airfoil drag coefficient were investigated. The simulation considered in free stream uniform velocity of (25 m/sec) at standard atmospheric pressure. The results showed that using a cylinder with diameter equal to leading edge diameter causes more pressure drop as the tandem gap decreased, noticing that this effect becomes more significant at a high angle of attack. A valuable reduction in drag coefficient of this configuration is achieved and it becomes more with a smaller cylinder diameter with respect to gap distance.

KEYWORDS

symmetric airfoil, tandem cylinder, variable gap, Drag evaluation

1. INTRODUCTION

The tandem gap of Bluff bodies in certain conditions contributes the flow field drag reduction, this reduction depends on several parameters such as the flow velocity range, the bodies' configuration, and their tandem adjustment [1]. These criteria will specify the influence of the exerted forces and moments (including the drag force) on the bodies.

One of the common airfoils drag reduction methods is the insertion of a small circular cylinder in front of it having a size equal to or less than the leading-edge radius that is linearly-positioned with the airfoil chord line. This approach with certain flow conditions and the specified gap distance between the bodies will minimize the exerting forces and moments, including the drag force to a certain value depending on the airfoil angle on attack value and direction since it affects the drag pressure-fraction adversely.

Several types of research have been conducted on the drag reduction for several types of airfoils. Hussain carried out experimental testing of the boundary layer separation position when installing circular cylinder in the front of NACA 0012 leading edge airfoil exposed to high subsonic free stream velocity [2]. The investigation included the variation of the airfoil angle of attack from (0-20°), the cylinder is placed linearly with the chord line in a (1mm) gap in front of the airfoil having a radius greater than the L.E. radius. The results showed that when installing the cylinder, the separation angle of attack has advanced from (14°) to (20°). Also, the lift and drag coefficient variation with increased angle of attack becomes very capricious.

Marchevskii and Puzikova simulated numerically the flow pattern of two tandem circular airfoils with variable distance spacing by adopting several flow modes; two symmetric vortices, two asymmetric vortices, and single vortex behind the first airfoil using the LS-STAG method for Reynolds number range between (50-300) [3]. For each flow mode, the second airfoil drag coefficient is negative for small gaps and gradually becomes positive, but it remains less than the drag coefficient for the single airfoil.

Some researchers proposed inserting a micro-scale cylinder in front of the leading-edge curvature of wind turbine blade at stall condition as an effective method for regulating the flow separation [4]. They simulated the case using the shear stress transport K-ω turbulence model with the variation of the cylinder size and location, the results indicated that the microcylinder can prevent flow separation without affecting the stability of the turbine and also can increase the blade generated torque by adjusting the appropriate size and position that are relevant to the formed mode of the stall.

The influence of inserting rotating cylinder in the front of the airfoil on the Aerodynamics effectiveness has been carried out numerically by Abdulla and Hamoud, who studied the NACA 0012 symmetric unconventional variable angle of attack airfoil interfaced with rotational cylinder spaced horizontally at variable distances ranging from (0.1-0.8) from the chord length using the SST K- ω turbulence model considering the cylinder to the mainstream velocity ratio within (1-4) [5]. The simulation results indicated that the optimum cylinder/mainstream velocity ratio is (4) with two positioning gaps of (0.5) & (0.8) from the chord length, respectively. In addition, the rotating cylinder has affected the stalled airfoil by reducing the separated region and decreasing the drag coefficient for the airfoil at the same angle of attack.

Similar case configuration numerical solution is performed by Nazari using the detached eddy simulation turbulence model [6]. The solution was performed on the NACA 0024 unconventional airfoil with leading edge positioned clockwise-rotational cylinder. The lift is increased by 60% when the cylinder rotated (4) times higher than the main flow domain, and the stalling angle of attack increases by a maximum of 80 % for a corresponding free stream to the rotational velocity ratio up to (4).

The aim of the present research is to study some of the aerodynamic characteristics including the airfoil drag coefficient and the flow field pressure contours for the constant speed subsonic flow passing through the combination of circular cylinder and the NACA 0012 symmetrical airfoil inside square cross-sectional duct placed taking into consideration changing of the cylinder diameter and the gap separating the two bodies with different angle of attack of airfoil ranging from (5-20°). The numerical solution of the case will be performed using the realizable K-Ɛ turbulence model in the ANSYS FLUENT 2017 CFD software considering the constant inlet flow velocity of (25 m/sec) with isothermal flow condition.

2. CASE CONFIGURATION

Figure (1a) denotes the adopted case where two bodies combination are selected one of them is a cross flow oriented single circular cylinder of certain diameter as a fore-body followed by the NACA 0012 symmetrical airfoil as a rare body placed in tandem were suggested. The simulation is performed by selecting different cylinder sizes: the first with diameter equals to the airfoil leading edge diameter; and the second one is half its initial size.

3. GEOMETRY DESCRIPTION

A circular cylinder placed in front of NACA 0012 symmetrical airfoil shown in figures (1a&b), the airfoil base chord length is (0.25) and leading-edge radius of (0.05) in meters. This tandem bodies placed in a (1x1) m square cross-sectional duct and (3) meters in length. The NACA 0012 airfoil geometry sketched using the formula stated in Eq. (1) with the aid of Solidworks program [7]. For each angle of attack, the two bodies linear gap is changed from (0.05-0.1) in meters. Table (1) illustrates the geometry configuration adopted cases for the CFD simulation denoting the airfoil adjusting angle of attack with assigned gap.

$$Y(x) = 0.6\left[0.27\sqrt{x} - 0.126x - 0.35x^2 - 0.29x^3 - 0.1x^4\right] \quad (1)$$

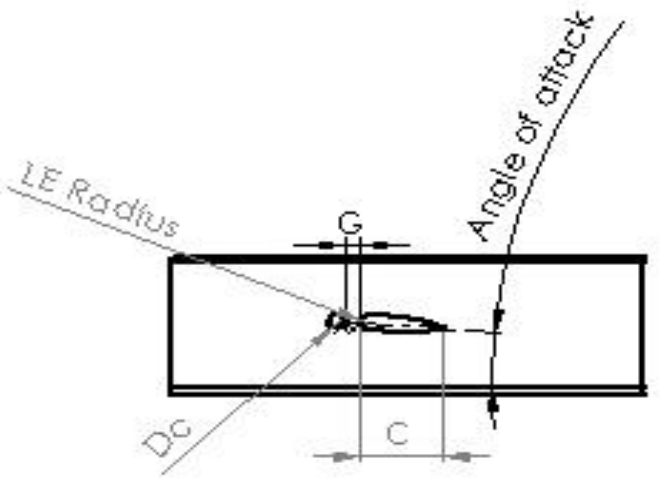

Figure 1a: The adopted case configuration

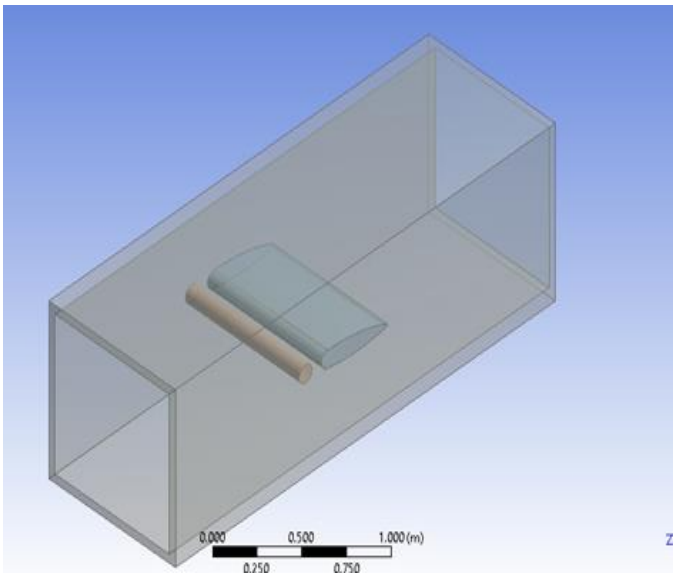

Figure 1b: The simulated case geometry

Table 1: Airfoil/ Cylinder Configuration Simulated Cases

Dc/LE Radius	G	Air foil Angle of Attack (Degree)
1	0.05	(5-20) In Positive clockwise direction
	0.075	
	0.1	
0.5	0.05	(5-20) In Positive clockwise direction
	0.075	
	0.1	

4. MATHEMATICAL MODELLING

4.1 THE GEOMETRY MESHING

The selection of the tetrahedron meshing method to the descriptive geometry is performed considering the proximity and curvature size function and applying smooth transition with maximum adopted layers of (10), and fine relevance center with fast transition method setting the growth rate to (1.10) and the maximum/minimum cells sizes to (0.3/0.0025) in meters, the total obtained nodes and cells account for the mesh were (24000) and (1300000), respectively. Figure (2) represents the meshed geometry for one of the adopted cases.

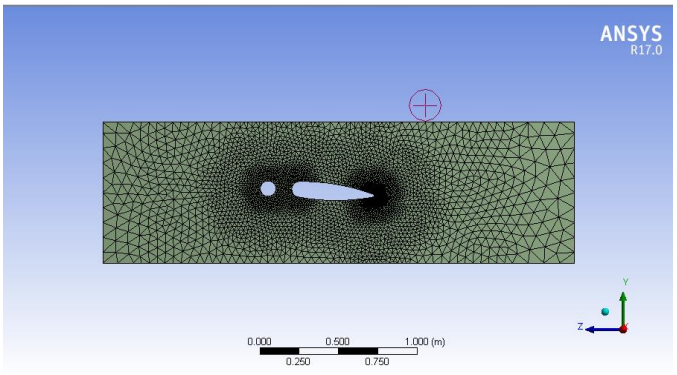

Figure 2: The generated mesh for the flow domain

4.2 The adopted turbulence model

The recently developed realizable K-Ɛ turbulence given in equations (2) & (3) is utilized for the numerical solution of the flow domain.
The transport kinetic energy differential equation:

$$\frac{\partial}{\partial t}(\rho K) + \frac{\partial}{\partial x}(\rho U K) = \frac{\partial}{\partial x}\left[\left(\mu + \frac{\mu_t}{G_K}\right)\frac{\partial K}{\partial x}\right] + G_a + G_b - \rho\mathcal{E} - Y + Sk \qquad (2)$$

Two major improvements were applied, the rate of dissipation transport equation is modified as follows:

$$\frac{\partial}{\partial t}(\rho\mathcal{E}) + \frac{\partial}{\partial x}(\rho U\mathcal{E}) = \frac{\partial}{\partial x}\left[\left(\mu + \frac{\mu_t}{G_{\mathcal{E}}}\right)\frac{\partial \mathcal{E}}{\partial x}\right] + \rho C_1 S_{\mathcal{E}} - \rho C_2 \frac{\mathcal{E}^2}{K+\sqrt{v\mathcal{E}}} + C_{1\mathcal{E}}\frac{\mathcal{E}}{K}C_3 G_b + S_{\mathcal{E}} \qquad (3)$$

And the turbulent viscosity is represented by the mathematical formula given by the equation:

$$\mu_t = \rho * c_\mu * \frac{K^2}{\mathcal{E}} \qquad (4)$$

4.3 The applied boundary conditions

The free stream flow velocity is considered uniform and uniform to the surfaces of the walls which are considered as smooth and stationary with non-slip condition with the adjusting the velocity of (25 m/sec) that means the flow is a highly subsonic state. The flow through and outside the tunnel is considered isothermal setting the exit boundary condition to the atmospheric pressure value.

4.4 The solution technique

The medium intensity and viscosity choice is considered for the turbulent flow domain solution with the application of the SIMPLE solution algorithm for the velocity and the pressure coupling solving, the upwind second-order advection is adopted for the momentum, and the K-Ɛ equations assuming the case is in the steady-state condition setting the convergence equation residual to (1e-3). The airfoil drag coefficient evaluation is obtained through the iterative solution monitoring and ticking the convergence detected value.

5. RESULTS AND DISCUSSION

5.1 The pressure contours

The flow pressure distribution contours around the tandem bodies in the mid-span location, with the pre-specified gap range with the adjusted airfoil angle of attack and cylinder diameter equal to the LE diameter illustrated in the following figures. Figures (3a, 3b, 3c) shows the P-contour for the positive value of the airfoil angle of attack (5), gap ratio (0.05-0.1). It is clear that the closer gap produces more stable pressure from the trailing edge and downstream the airfoil, in addition, the pressure gradient at the upper and lower surfaces of the airfoil profile has slightly decreased due to the effect of the turbulence wakes produced by the cylinder body.

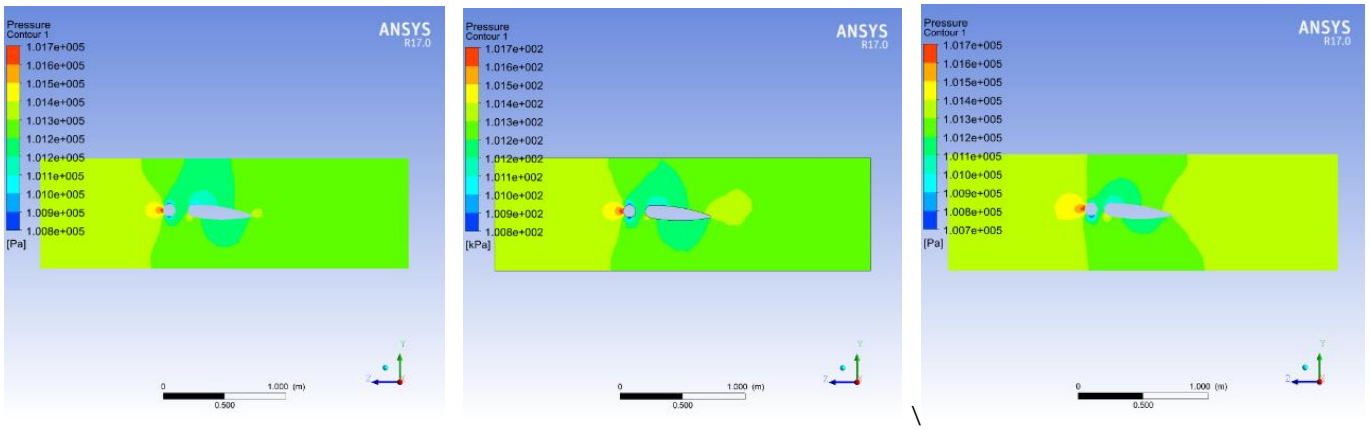

(a) **(b)** **(c)**

Figure 3: Airflow pressure contour for G (0.1-0.05) at (+5) angle of attack

When the airfoil leading edge is raised to (10°), as presented in Figures (4a,4b,4c), the pressure disturbances is increased especially for the lower airfoil surface developing stagnation region at the LE curvature. Furthermore, a gradual step down in the pressure gradient results on both the airfoil surfaces which means that the airfoil angle of attack has increased the flow disturbances due to the adverse pressure effect this lead to a conclusion that the decreased gap is generating slightly accelerated flow that will retract the stall phenomena.

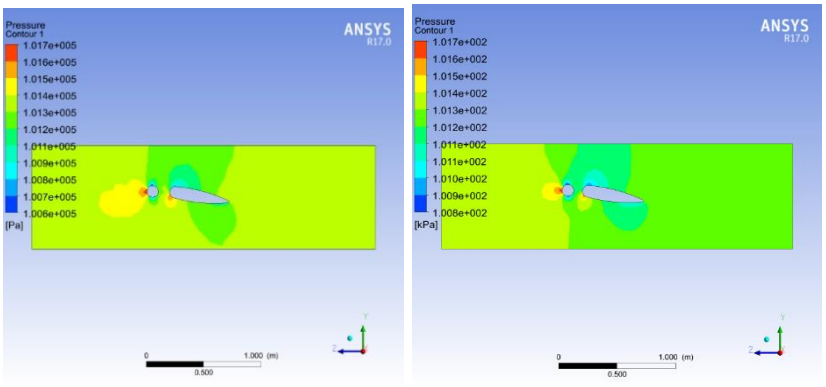

(a) (b)

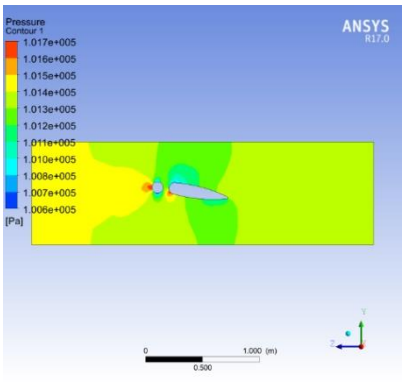

(c)

Figure 4: Airflow pressure contour for G (0.1-0.05) at (+10) angle of attack

Further increment in the angle of attack approaching the stall condition results presented in figures (5a, 5b, 5c), the stagnated region eliminated with further step-down for the resulted pressure.

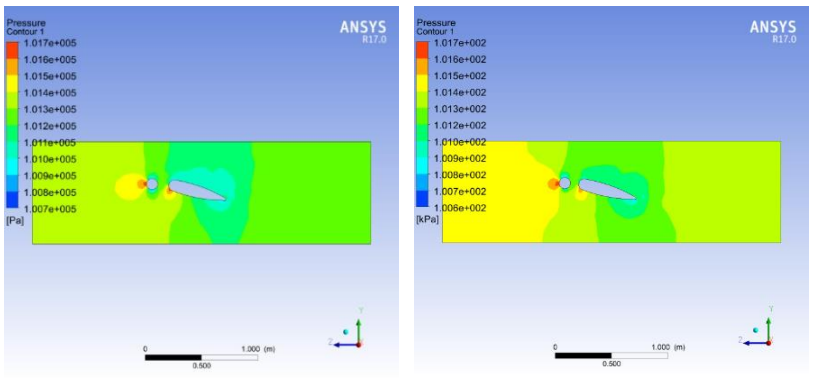

(a) (b)

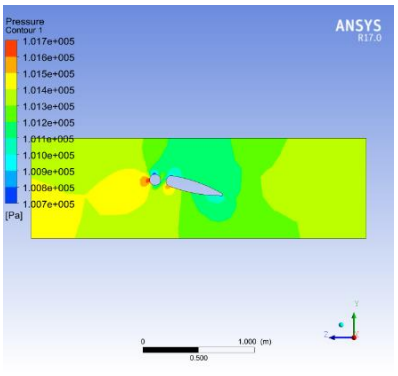

(c)

Figure 5: Airflow pressure contour for G (0.1-0.05) at (+15) angle of attack

When the flow exceeds the stall condition with (α=20°), the cylinder gap accelerating effect is obvious from figure (6a, 6b, 6c) noticing a rapid decrease in the resulting pressure, especially for the airfoil upper surface.

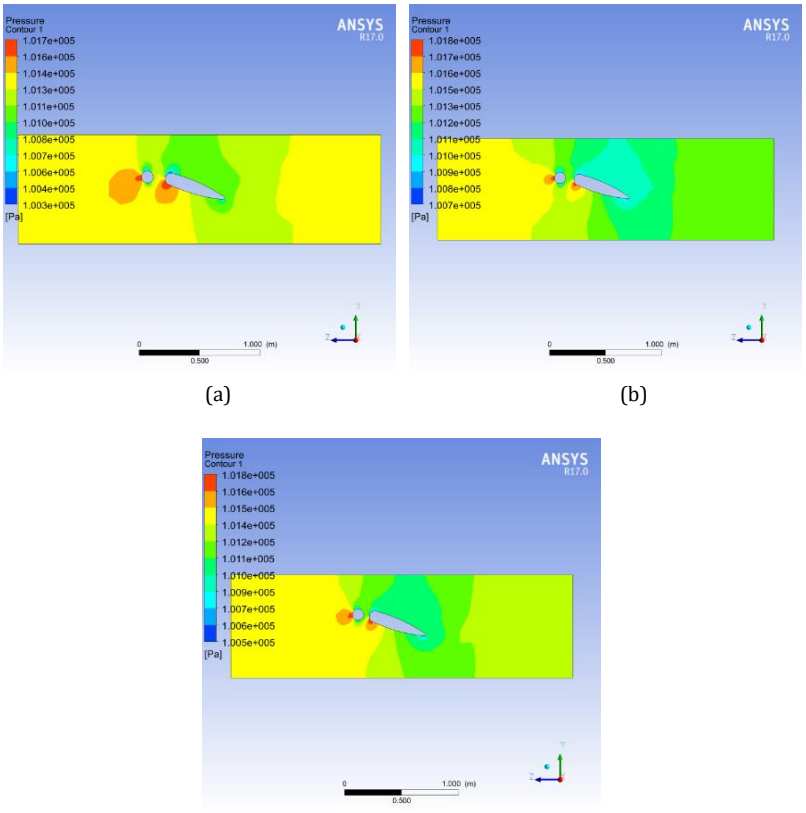

Figure 6: Airflow pressure contour for G (0.1-0.05) at (+20) angle of attack.

Decreasing the cylinder size with the same approaching gap criteria has a smaller effect on the pressure contours for the small angle of attack (α=5&10°) in Figures (7a, 7b, 7c) and (8a, 8b, 8c). When comparing the results with larger cylinder diameter for the same angle of attack, it is clear that the smaller cylinder is producing less wakes behind it, which leads to more developed pressure contours around the airfoil.

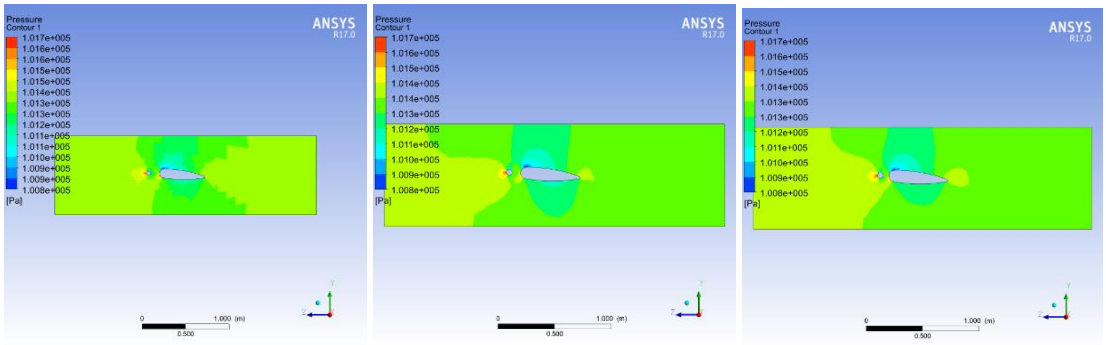

Figure 7: Airflow pressure contour for G (0.1-0.05) at (α=+5) for D_C=0.5 LE diameter

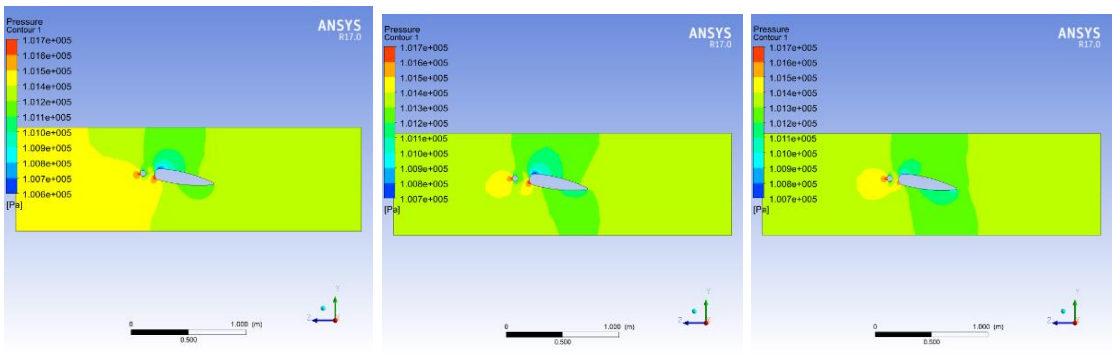

Figure 8: Airflow pressure contour for G (0.1-0.05) at (α=+10) for D_C=0.5 LE diameter

For higher sloping airfoil and cylinder arrangement illustrated in figures (9a, 9b, and 9c), the closest tandem distance will further increase the pressure with a higher rate for the lower airfoil surface concluding that smaller cylinder that approaching the airfoil has an adverse effect on the resulting flow

field pressure at high airfoil slope angle.

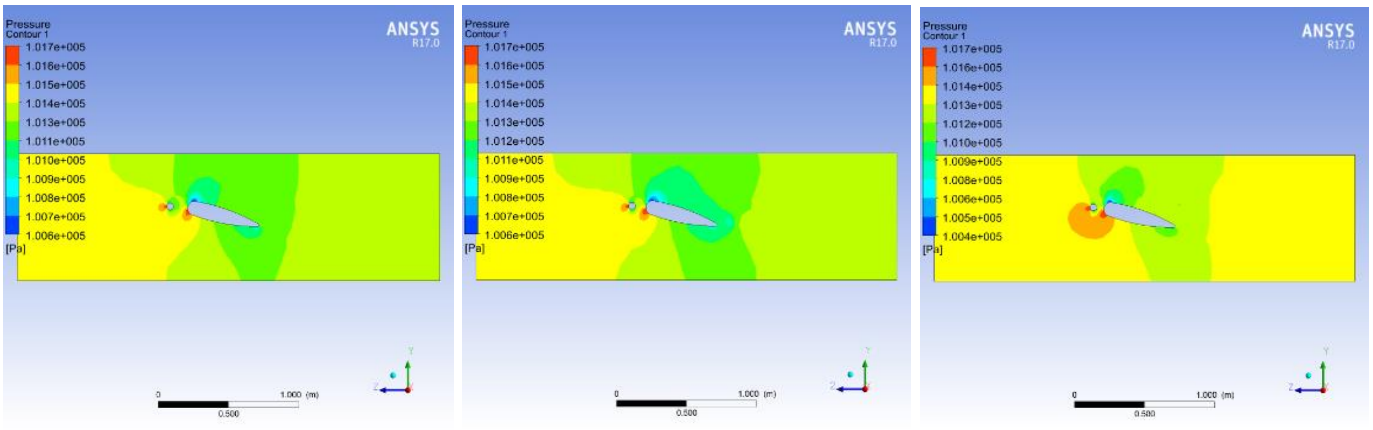

(a) **(b)** **(c)**

Figures 9: Airflow P-contour for G (0.1-0.05) at (α=+15) for D_C=0.5 LE diameter

5.2 The airfoil drags coefficient results

From the pre-discussed simulation results for the flow pressure distribution, the simulation of the evaluated airfoil drag coefficient for each angle of attack at the specified tandem bodies gap for each cylinder diameter, plotted in figures (10&11).

Figure (10) represents the drag coefficient variation at increased angle of attack with the assigned cylinder gap with respect to the stand-alone NACA0012 (without cylinder). It shows that the Cd gradual rise with the angle of attack noticing the sudden drop is still occur after the default stall angle of (14°) in spite of introducing a cylinder. The decreasing of Cd is clear due to the cylinder interaction effect. The decreased of gap distance has a negative effect on the drag denoting the high jump in its value when the gap is reached (0.05). The effect of inserting the cylinder in the front of the airfoil has significantly reduced the drag coefficient for less than its half basic value especially near the stall condition.

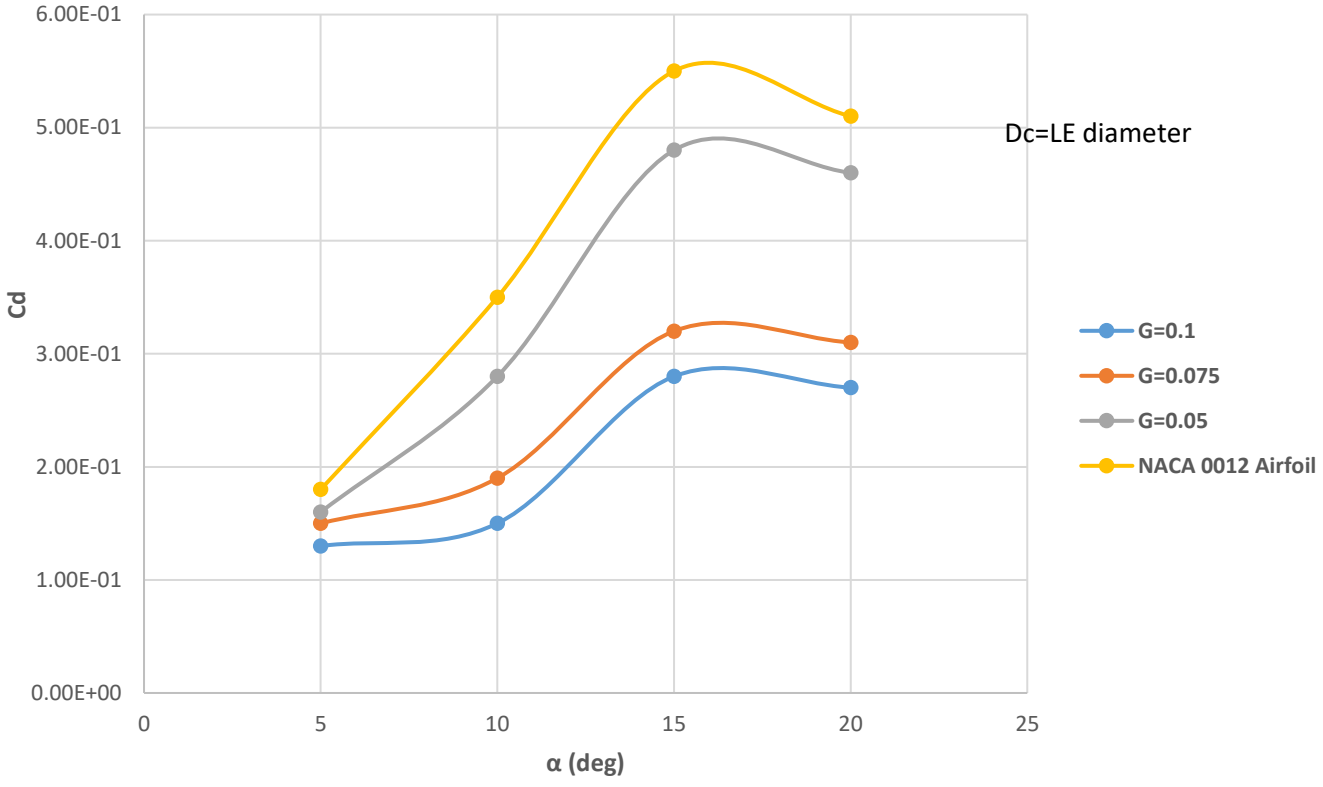

Figure 10: Drag coefficient variation for the airfoil with increased angle of attack

For the cylinder diameter of (1/2 of its basic size), the evaluated drag coefficient for the same simulated cases (angle of attack and gap distance), are shown in figure (11). The most important result is that the cylinder utilization with reduced diameter to its half original size has significantly caused higher drop down in the drag value reaching its quarter initial value without inserting the cylinder.

The reduced drag values and further retraction in the default stall angle leading to a conclusion that the larger cylinder diameter with closer gaps at moderate turbulent flow speed will increase the drag coefficient at high inclined airfoil.

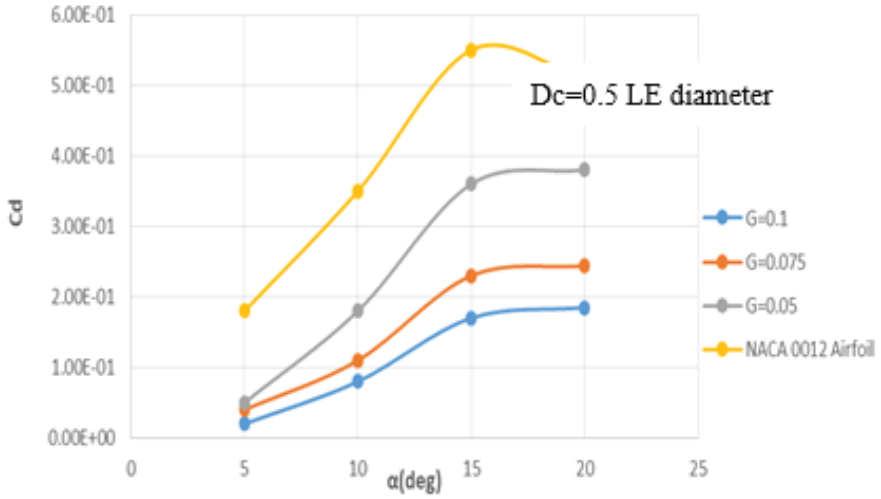

Figure 11: Drag coefficient variation for the airfoil with increased angle of attack

6. SOLUTION VALIDATION

The utilized numerical solution technique for the prescribed flow case verification is obtained by comparing the obtained results with the calculated drag coefficient for the NACA 0012 airfoil experimental tests performed. The airfoil chord and span dimensions were modified to match the profile of the tested blade in addition to the cylinder size and position. Table (3) shows that the percentage error in the drag coefficient is between (10-18) %, respectively.

Table 2: Comparison with experimental results

Angle of attack	Calculated Cd	Experimental Cd
5	0.12	0.1
10	0.23	0.21
15	0.27	0.24
20	0.75	0.65

7. CONCLUSIONS

The cylinder size has an obvious effect on the flow field pressure contours noticing that the large cylinder size contributes in flow acceleration at stalling condition that is increased with smaller assigned bodies' gap. The smaller cylinder size has a minor effect on the flow pressure distribution at small angles of attack, while it forms a major concern for stalled flow condition remaking increased flow pressure as much as the tandem bodies are closer. The inserting of circular cylinder in the front of the airfoil has reduced the airfoil drag by a variable rate that is arises with the increased angle of attack depending on the cylinder size.

The NACA 0012 airfoil drag reduction is more significant when the adjusted cylinder size is Dc=0.5 LE diameter reaching to its quarter initial value without utilizing the cylinder.

For low airfoil angle of attack (5°), the airfoil drag coefficient change is small for the cylinder initial size but becomes more effective with increased airfoil angle of attack and increased gap clearance reaches 0.1. For small cylinder size, the stall angle has been retracted above its default value by (5°) for the NACA 0012 airfoil.

Nomenclatures	
Cd	Drag coefficient
C_1, C_2, C_ε	Turbulent model constants
Dc	Cylinder diameter, m
G_a, G_b	Turbulent kinetic energy generation due to velocity gradient and buoyancy
K	Kinetic energy of turbulence,
U	Velocity vector, m/sec
Sk, Sε	Source term for K and ε equations
Y	Fluctuation diffusion in turbulence
Greek Symbols	
□	The angle of attack, deg.
ρ	Fluid density, Kg/m^3
μ	Dynamic viscosity, kg/m.sec
ε	The rate of dissipation of kinetic energy
$\sigma_{□□}\sigma_\varepsilon$	Turbulent model constants
Abbreviations	
LE	Airfoil leading edge
NACA	National Advisory Committee for Aeronautics

REFERENCES

[1] Charles, T., Lu, Y., Yang, Z. 2017. Impact of the gap size between two bluff bodies on the flow field within the gap. 13th Int. Conf. of Heat transfer, Fluid Mechanics and Thermodynamics.

[2] Hussain, G.F.M. 2010. The effects of the cylinder at the leading edge of airfoil NACA 0012 on the boundary layer separation. Alkufa Engineering Journal, 1 (2), 73-88.

[3] Marchevskii, I.K., Puzikova, V.V. 2016. Numerical Simulation of the Flow around Two Fixed Circular Airfoils Positioned in Tandem Using the LS-STAG Method. Journal Of Machinery Manufacture And Reliability, 45 (2), 130-136.

[4] Wang, Y., Li, G., Shen, S., Huang, D., Zheng, Z. 2018. Investigation of Aerodynamic performance of horizontal axis wind turbine by setting micro-cylinder in front of blade leading edge. Energy, 143, 1107-1143.

[5] Abdulla, N.N., Hamoud, A.J. 2014. Numerical Study of Optimum Configuration of Unconventional Airfoil with Steps and Rotating Cylinder for Best Aerodynamics Performance. Journal of Engineering, 6 (20), 179-199.

[6] Nazari, N. 2015. Control of flow past an airfoil section using rotating cylinders. M.Sc. Thesis. American University of Sharjah, UAE.

[7] Lin, Y.F., Lam, K., Zou, L., Liu, Y. 2013. Numerical study of flow past airfoils with wavy surfaces. Journal of Fluids and structures, 36, 136-148.